# Printable hyaluronic acid hydrogel functionalized with yeast-derived peptide for skin wound healing

[a]Pejman Ghaffari-bohlouli, [a]Julia Simińska-Stanny, [a]Hafez Jafari, [abc]Mahta Mirzaei, [d]Lei Nie, [e]Christine Delporte, [a]Amin Shavandi*

[a] Université libre de Bruxelles (ULB), École polytechnique de Bruxelles-BioMatter unit, Avenue F.D. Roosevelt, 50 - CP 165/61, 1050 Brussels, Belgium

[b] Department of Environmental Technology, Food Technology and Molecular 11 Biotechnology, Ghent University Global Campus, Incheon, South Korea

[c] Department of Food Technology, Safety and Health, Faculty of Bioscience Engineering, 14 Ghent University, Coupure Links 653, 9000 Ghent, Belgium

[d] Key Laboratory of Molecular Target & Clinical Pharmacology and the State & NMPA Key Laboratory of Respiratory Disease, Key Laboratory of Molecular Target & Clinical Pharmacology and the State Key Laboratory of Respiratory Disease, School of Pharmaceutical Sciences & the Fifth Affiliated Hospital, Guangzhou Medical University, Guangzhou, P.R. China, College of Life Sciences, Xinyang Normal University, Xinyang 464000, China

[e] Laboratory of Pathophysiological and Nutritional Biochemistry, Medical School, Université Libre de Bruxelles, Route de Lennik, 808 – CP611, Brussels 1070, Belgium

* Corresponding authors: Email: amin.shavandi@ulb.be, Tel: +326503681

**Abstract**

Targeted delivery of bioactive agents, growth factors, and drugs to skin wounds is a growing trend in biomaterials development for wound healing. This study presents a printable hyaluronic acid (HA) based hydrogel to deliver yeast-derived ACE-inhibitory peptide of VLSTSFPPW (VW-9) to the wound site. We first conjugated tyramine (Ty) on the carboxyl groups of the HA to form a phenol-functionalized HA (HA-Ty); then, the carboxylic acid groups of HA-Ty were aminated with ethylenediamine (HA-Ty-$NH_2$). The primary amine groups of the HA-Ty-$NH_2$ could then react with the carboxylic acids of the peptide. The hydrogel was then 3D printed and crosslinked with visible light. The modification of HA was confirmed by $^1$H NMR and FTIR. The swelling capacity of the conjugated hydrogels was 1.5-fold higher compared to the HA-Ty-$NH_2$ hydrogel. The conjugated peptide did not affect on rheological properties and morphology of the hydrogels. The 3T3-L1 fibroblast cells seeded on the peptide-modified hydrogels exhibited higher viability than the hydrogels without the peptide, indicating that the peptide-enriched hydrogels may have the potential for wound healing applications.

Keywords: wound healing; hydrogel; 3D print; photocrosslink; peptide

**Graphical abstract**

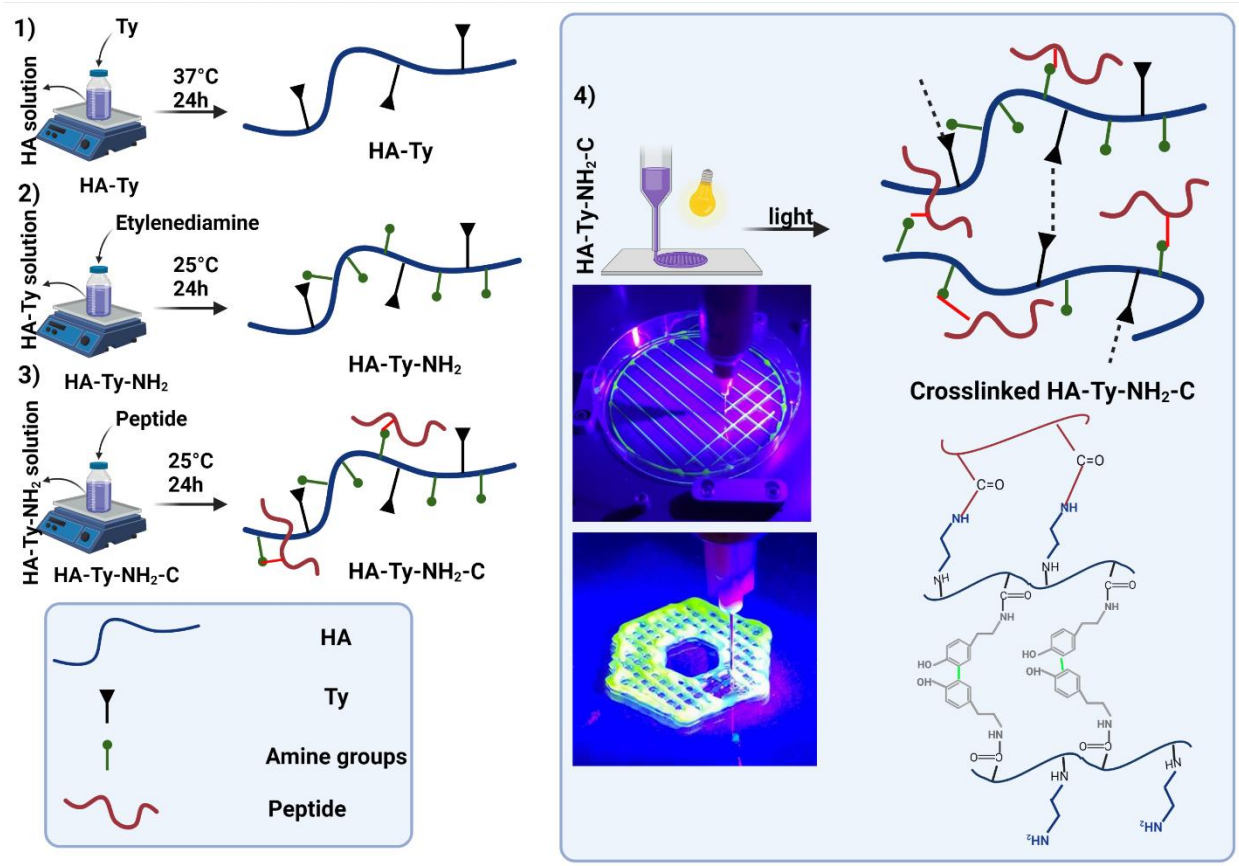

## 1 Introduction

Certain peptides can act as regulators for enzyme activity which are responsible for directing various cellular reactions and metabolic pathways. The high specificity of peptide sequences and their ability to inhibit functions of particular enzymes renders them effective bio-stimulants and regulators of enzyme-driven processes [1, 2]. Arginylglycylaspartic acid (RGD) is a commonly reported tri-amino acid sequence peptide motif for conjugation onto biomaterials to enhance cell adhesion and proliferation [3-5]. The beneficial effect of other short peptide sequences, such as Nap-GFFKH Ac-ILVAGK-NH2 and Ac-LIVAGK-NH2, for the healing of full-thickness excision and burn wounds were also reported [6, 7]. VW-9 peptide with the angiotensin-converting enzyme (ACE) reducing activity is responsible for blood pressure moderation. The ACE-inhibitory activity of the peptide of VLSTSFPPW (VW-9) was confirmed in our previous studies [8, 9], reporting that the VW-9 acted as a non-competitive inhibitor and bound with equal affinity to the ACE enzyme and substrate-enzyme complex [10]. Additionally, given that no amino acids in the active site of ACE were involved in the interaction with VW-9, it can be hypothesized that the impact of this sequence on ACE function can be more predictable and efficient in terms of blood pressure regulation. Therefore VW-9 peptide may be a potential candidate to lower blood pressure at the site of the wound and stimulate the healing processes in the wound bed [10, 11].

Hydrogels with tunable structure and high hydrophilicity that can maintain skin hydrated, support the debridement of the necrotic tissue, and prevent infection have the potential to mimic the properties of tissue extracellular matrix (ECM), facilitating remodeling and wound healing [12-14]. It has been reported that the presence of certain drugs, growth factors, minerals, antibacterial agents, and bioactive peptides improves the performance of hydrogels as wound dressings [15-17].

Natural polymers can be co-assembled with short peptides and form hydrogels under various conditions [3, 18, 19]. Polysaccharides such as hyaluronic acid (HA), chitosan, heparin, and alginates have been used to increase the adhesion of peptide-based materials [18, 20]. However, the lack of control over the release of the peptides is one major drawback [21]. Therefore, there is a need for localized and sustained delivery of the peptides which can be met through chemical or physical interaction between peptides and hydrogels to prolong the release and enhance the peptide activity [21-23]. Among the natural polymers, HA is an essential component of skin tissue repair and healing. HA is a naturally occurring substance found in the body that plays a critical role in the health and appearance of the skin. It is a substance that helps to bind cells together, keep moisture in the skin, and provide structural support to the skin. Additionally, HA helps to keep the skin supple and soft and can help to reduce the appearance

of scars from injury or surgery. HA also helps to promote the production of collagen. Finally, HA is essential for the healing of wounds. It helps to promote the growth of new skin cells and helps to reduce inflammation and pain associated with injury [24, 25]. In our previous study [26], we showed the potential of VW9 peptides for skin wound healing. In this study, our objective is to develop a 3D printable HA-based biomaterial, modified with the VW9 bioactive peptide with potential use as a wound dressing. To achieve this, HA was modified with ethylenediamine to provide free primary amine on the HA backbone for conjugation with carboxylic groups of the VW-9 peptide. It was hypothesized that slow release of the peptide via degradation of modified HA hydrogel would supply the peptide during the healing.

## 2 Materials and methods

### 2.1 Materials

Hyaluronic acid (HA) was purchased from Xi'an JKA Biotech Co., Ltd., China, with Mw of 299849 g/mol. Sodium persulfate (SPS) was from Sigma-Aldrich (St. Louis, MO, USA). Tyramine hydrochloride (Ty) was obtained from Biosynth (Berkshire, MA, USA). 4-(4,6-Dimethoxy-1,3,5-triazin-2-yl)-4-methylmorpholinium chloride (DMTMM) and deuterium oxide ($D_2O$) were purchased from Tokyo Chemical Industry (Tokyo, Japan). Riboflavin 5'-monophosphate sodium salt 73-79 % fluorometric (RF) was purchased from J&K (Pforzheim, Germany). Dulbecco's Modified Eagle Medium (DMEM), Trypsin/EDTA, Glutamine, Penicillin-streptomycin, fetal calf serum (FCS), DMEM with high glucose, Hoechst, and Ethidium homodimer were purchased from Thermo Fisher Scientific (Waltham, MA, USA).

### 2.2 Synthesis of HA-Ty

Ty was conjugated on the HA backbone as previously described with some modification [27]. Briefly, two g of HA was dissolved in 200 mL of deionized (DI) water under stirring (200 rpm) at 37°C. Then five mmol of Ty and five mmol of DMTMM were added to the solution [28] and the reaction was run for 24 h at 37°C. After the reaction was complete, the solution was dialyzed for four days at room temperature (25°C) with a 14 kDa cutoff membrane in distilled water with at least three changes per day. Following the dialysis, samples were poured into plastic dishes and frozen for three-four h before lyophilization for three days. The resulting dried product – tyramine conjugated hyaluronic acid (HA-Ty) was kept in a moisture-free desiccator until further use.

### 2.3 Synthesis of HA-Ty-$NH_2$

The substitution of carboxylic acid groups of HA-Ty with the primary amine of ethylenediamine was carried out following the previous methods [29, 30]. Initially, the remaining carboxylic acid groups of HA were calculated by subtracting the substitution degree of Ty from the initial HA carboxylic acid groups via $^1H$ NMR of HA-Ty; then a 30-equivalent excess of ethylenediamine according to the remaining

carboxylic acid groups was added into the aqueous solution of HA-Ty with a concentration of 0.5% w/v. The pH of the reaction mixture solution was adjusted to 6.5 by HCl (1M). 20-fold equivalent excess of EDC and NHS according to the remained carboxylic acid groups of HA-Ty were dissolved into the reaction mixture and stirred at 150 rpm for 24 h at 25°C. The mixture was dialyzed by a dialysis membrane 14 kDa against distilled water for three days, and the water was changed three times per day. To precipitate the HA-Ty-$NH_2$ powder, five g NaCl was dissolved into 100 mL of the dialyzed solution before the addition of 400 mL of 70% ethanol. The precipitated white powder was redissolved in water and lyophilized after dialyzing for three more days.

### 2.4 Synthesis of HA-Ty-$NH_2$-C (conjugated HA-Ty-$NH_2$)

The peptides were conjugated on the HA-Ty-$NH_2$ backbone by the reaction between the primary amine groups of HA-Ty-$NH_2$ and the carboxylic acids of the peptide and named HA-Ty-$NH_2$-C (Figure 1a). Initially, HA-Ty-$NH_2$ (1% w/v) was dissolved in phosphate buffer saline (PBS) containing 0.1% v/v of acetic acid. A 5-fold equivalent of NHS and EDS according to the equivalent of the primary amine groups of HA-Ty-$NH_2$ with a ratio of 1:1 (equivalent: equivalent) was added into the solution. An excessive amount of the peptide (300 mg (5-fold equivalent of the peptide according to the equivalent of the primary amine groups of HA-Ty-$NH_2$, which was calculated by integration of the peak related to conjugated ethylenediamine)) was dissolved in the solution and stirred at 150 rpm for two days at room temperature. The solution was dialyzed against distilled water for three days with two daily changes. The purified solution was lyophilized for 48 h and stored at -18°C until use.

### 2.5 Synthesis of HA-Ty-$NH_2$-B (Blended HA-Ty-$NH_2$)

To evaluate the effect of the conjugated peptide on various properties of HA-Ty-$NH_2$ including rheological properties, swelling, degradation, water retention, and cell viability, an equal amount of peptides with the amount of peptides that were conjugated on HA-Ty-$NH_2$ were blended with HA-Ty-$NH_2$ and named HA-Ty-$NH_2$-B. The amount of conjugated peptide on HA-Ty-$NH_2$ was measured by the BCA protein assay kit [31] (at 32.7 µg/mg (3.27%)).

### 2.6 Hydrogel formation

HA-Ty-$NH_2$, HA-Ty-$NH_2$-B, and HA-Ty-$NH_2$-C hydrogels were prepared via photocrosslinking of the conjugated Ty on HA induced by Riboflavin and visible light irradiation at room temperature and limiting the access of the light based on previous studies [27, 32]. Briefly, according to the molecular weight of each sequence of the synthesized HA-Ty-$NH_2$ with or without peptide, solutions of three% w/v of HA-Ty-$NH_2$, HA-Ty-$NH_2$-B, and HA-Ty-$NH_2$-C were prepared. Then, 0.001g of RF and 0.047g of SPS per one mL of

the solutions were added and vortexed to reach the final concentrations of two mM and 20 mM, respectively. The photocrosslinking was achieved by irradiating the solutions with a visible light source with a power of 2500 mW/cm$^2$ at 440nm for the 60s. RF in the exposure to visible or UV light by absorbing the photon energy excites to $^1$RF*, which is unstable with a short lifetime ($10^{-8}$s)[27]. The singlet RF transfer to a highly reactive $^3$RF* with a more lifetime ($10^{-2}$s). The $^3$RF* is an oxidant biradical that can generate reactive singlet oxygen ($^1O_2$) via energy transformation to $O_2$ or generate radical ions and free radicals via reaction with solvents and other substrates[27]. SPS as an oxidizing agent and is used as a catalyst in the photo crosslinking with RF. SPS dissociates into radicals and $SO_4^{-2}$ in presence of the $^3$RF* helps to speed up the reaction by supplying electron to the reaction and acts as a co-initiator to crosslink the phenol moieties. Then, the crosslinked hydrogels were kept overnight to complete the crosslinking reaction [27].

### 2.7 Hydrogel Characterization

$^1$H NMR analyses of the hydrogels were performed at 25°C using a 400 MHz Varian INOVA spectrometer with $D_2O$ as the solvent to confirm the conjugation of Ty, ethylenediamine, and the peptide on HA and to determine the substitution degree of synthesized polymers (HA-Ty, and HA-Ty-$NH_2$). The $^1$H NMR spectra for 10 mg/mL of the polymers in $D_2O$ were recorded, and the NMR data processing (Fourier transform, phase correction, baseline correction, and chemical shift referencing of the spectrum) was performed using MestReNova x64 software [33, 34]. The infrared spectra of the HA, HA-Ty, HA-Ty-$NH_2$, HA-Ty-$NH_2$-B, HA-Ty-$NH_2$-C, and the peptide were determined using the FT/IR-6600 spectrometer (JASCO, Japan) with a resolution of 4 cm$^{-1}$ and 64 scans per spectrum. The morphology of the cross-section of the hydrogels and the effect of the peptide on the structure of the hydrogels were evaluated using scanning electron microscopy (SEM) (HITACHI, SU-70, Japan).

### 2.8 Physical parameters of the hydrogels

The yield of HA-Ty-$NH_2$, HA-Ty-$NH_2$-C, and HA-Ty-$NH_2$-B hydrogels was measured by comparing the initial wet weight of each sample (Mi) and their dried weight (Md) after incubation in an oven at 40°C for four days via following equation [35].

$$Yeild(\%) = \frac{\mathrm{Md}}{\mathrm{Mi}} \times 100 \quad (1)$$

The swelling behavior of the hydrogels was investigated by changing the weight of the hydrogels during incubation in PBS with a pH of 7.4 at 37.5°C. For this purpose, 100mg of the hydrogels were incubated into 10 mL of the buffer (Wi), and then at pre-determined time points (0, 1, 2, 3, 5, 10, 24, 48,

and 72 h), the weight of the hydrogels was measured again after removing the surface water by paper tissue (Wd). The percentage of capacity of the hydrogels to uptake water was calculated using equation two[36].

$$Swelling\ (\%) = \frac{(Wd-Wi)}{Wi} \times 100 \quad (2)$$

To measure the water retention ratio, 50mg of the dried hydrogels were incubated in the buffer (PBS with pH of 7.4) at 37.5°C for two days to swell completely. The fully swelled hydrogels were separately placed into a 24-wells plate and left at room temperature to evaporate their water. At pre-determined time points (0, 1, 2, 3, 5, 10, 12, and 24 h), after absorbing the water on the surface of the hydrogels were weighted (Mt). Then the hydrogels were transferred into an oven at 60°C for four days to dry and reach a constant weight (M0). Finally, according to equation three, the hydrogels' water retention percentage was calculated[35].

$$Water\ retention\ ratio\ (\%) = \frac{(Mt-M0)}{M0} \times 100 \quad (3)$$

The hydrolytic degradation was assessed as follows. The weight loss behavior of the hydrogels was studied by comparing the weight of the hydrogels after soaking in PBS (pH of 7.4) at 37.5°C for three days (to absorb water (Mi) fully) and the weight of the hydrogels after each time point (0, 1, 2, 3, 4, 5, 6, and 7 days) (Md). At each time point, the hydrogels were taken out from the PBS and placed in an oven at 40°C for four days to dry. The degradation percentage of each hydrogel was calculated via the following equation[35].

$$Hydrolytic\ degradation(\%) = \frac{(Mi-Md)}{Mi} \times 100 \quad (5)$$

The porosity of the HA-Ty-$NH_2$, HA-Ty-$NH_2$-B, and HA-Ty-$NH_2$-C hydrogels was measured by the liquid displacement method [37]. A known mass of the freeze dried hydrogel sample was placed into a graduated cylinder containing a known volume (V1) of ethanol for five minutes. The total volume (V2) of the ethanol and sample was recorded, then the sample was removed and the volume (V3) of the remaining ethanol was recorded. Three replicates were taken for each sample and porosity was calculated using equation 6.

$$\text{Porosity} = \frac{V_1-V_3}{V_2-V_3} \times 100 \quad (6)$$

## 2.9 Rheological investigation

The viscoelastic properties of the hydrogels with and without peptide were studied using a rheometer (Anton Paar MCR 302, Austria) equipped with a plate-plate geometry (25 mm) at 37°C. Oscillatory tests were performed to determine the effect of peptide incorporation on the storage modulus (G') and loss modulus (G") of the hydrogels [38]. The hydrogel precursors (300 µl) were deposited on the rheometer plate, and the photocrosslinking using visible light was performed before the experiment. First, a frequency sweep test (0.1-10 Hz) was carried out with a constant strain of 0.1%. Moreover, the linear viscoelastic region of (LVR) was determined by an amplitude sweep test (1-1000%) at a constant frequency of 1Hz.

To investigate the effect of photocrosslinking, the viscosity of the HA-Ty-$NH_2$, HA-Ty-$NH_2$-B, and HA-Ty-$NH_2$-C solution and hydrogels were evaluated between shear rates of 0.001 to 1000 1/s using a rheometer (Anton Paar MCR 302, Austria) equipped with a plate-plate geometry (25 mm) at 25°C.

## 2.10 Peptide release measurements

To study the release rate of the peptide from HA-Ty-$NH_2$, HA-Ty-$NH_2$-C, and HA-Ty-$NH_2$-B hydrogels by BCA protein assay kit [31], 100mg of the hydrogels were incubated into PBS (pH of 7.4) at 37.5°C. At pre-determined time intervals (0, 1, 2, 3, 4, 5, 6, 12, 24, 48, 72, 96, 120, and 144 h), 50µl of the media was transferred into 1.5 mL microcentrifuge tubes containing 200µL of cold acetone (-20°C). The mixture was vortexed, incubated at -20°C for 30min, and centrifuged at 14000 rpm for 10min. The supernatants were decanted, and the tubes were placed at room temperature for 30 minutes to evaporate the remaining acetone. The peptide pellets were dissolved into 50 µL of DI water by vortex and subjected to BCA protein assay. The concentration of the released peptides was calculated using a standard curve. The cumulative release of the peptides from HA-Ty-$NH_2$-C and HA-Ty-$NH_2$-B was calculated according to the following equation[39].

$$E = \frac{V_E \sum_1^{n-1} C_i + V_0 C_n}{m_0} \times 100\% \quad (6)$$

Where the E is the cumulative release of the peptides (%), $V_E$ is the volume of the withdrawn release media (50µL), $V_0$ is the initial volume of the release media, and $C_n$ and $C_i$ are drag concentrations (µg/mL) at the sampling time i and n, and $M_0$ is the initial mass of peptides in the hydrogels. The release rate of peptides from the hydrogels was investigated in triplicate.

### 2.11 Cell culture and cell seeding

Fibroblast cells (3T3-L1) were grown as previously described [36, 40]. All powder-like reagents, including Riboflavin, SPS, HA-Ty-$NH_2$, HA-Ty-$NH_2$-C, and HA-Ty-$NH_2$-B, were sterilized by UV for 2h before reconstitution in sterilized HBSS [41, 42]. All other solutions were sterile-filtered. Hydrogel samples of 50 µL volume were placed in 96-well plates or Millicell EZ SLIDE 8-well glass (Merck, Kenilworth, NJ, USA) and incubated for one day in DMEM. The next day, 5 x $10^3$ cells in 20µl of cell culture medium were placed on the hydrogel after removing DMEM, followed by filling wells with a new cell culture medium. Samples were placed in a cell incubator (37°C, 5% $CO_2$) for the next 1, 3, and 7 days and the cell culture medium was changed daily.

### 2.12 Cell viability and staining

To estimate the viability of 3T3-L1 seeded on the surface of the hydrogels, samples were treated with the CellTiter 96® AQueous One Solution Cell Proliferation Assay (MTS, Promega) [40]. On days 1, 3, and 7, cell media was removed from the wells, followed by the addition of 100 µL of DMEM and 15 µL of MTS reagent, and incubation at 37°C for 3h. After the reaction, the supernatant was recovered and transferred into another 96-well plate and read at 492 nm (Epoch, BioTek®, USA). The cell viability was calculated over time (1, 3, and 7 days) in relation to the experiment control (HA-Ty-$NH_2$ hydrogel) (viability equal to 100%) to normalize the absorbance of each experimental group [43]. To investigate the distribution of cells on the hydrogels, LIVE/DEAD staining with Hoechst and Ethidium homodimer was performed. For this purpose, the samples on day five were washed with warm DPBS and incubated with ethidium homodimer-1 (10 µM) and Hoechst (10 µg/mL) at 37 °C for 45 min. After washing the samples with DPBS and cell fixation with paraformaldehyde (PAF, 4%), the cell viability of the hydrogels was observed through a fluorescent microscope (ZOE, Biorad, Hercules, CA, USA), in which the live cells were blue and dead cells were red. Micrographs were randomly taken during hydrogel observation.

### 2.13 Printability

To demonstrate the printability of the hydrogels, the hydrogel precursor was transferred into a 10 mL UV-shielded syringe. A GeSim BioScaffolder 3.2 (Germany), a pneumatic-based extrusion printer, was employed to deposit the material on the surface of a culture dish according to a pre-designed pattern. The hydrogel precursor was pneumatically extruded through the 25G metallic nozzle employing a pressure of 20 kPa and a speed of eight mm/s. Extruded strands of the hydrogel were subjected to visible light photocrosslinking (Dymax, VisiCure, Mavom, Belgium) at a power of 2500 mW/$cm^2$ at 440nm immediately after deposing onto a Petri dish. Printed 3D hydrogels were cured for one min following the printing process to obtain stable hydrogel printouts. The printability of the hydrogel precursors (25G nozzle, speed

10 mm/s, pressure ~ 20 kPa) without and with peptide (both blended and conjugated) was investigated utilizing the in-situ crosslinking approach. To quantitively determine the printability, the hydrogels were printed into grid patterns (20 x 20 mm) or parallel lines, photographed with a scale bar, and the perimeters of three different inner squares and diameters of the lines (n=3) were measured using ImageJ (NIH, USA) [44]. Gathered values were used to quantitively determine pore squareness, based on the circularity of the pores inside of a grid – Ps (equation 7) [45, 46].

$$Pore\ squareness = \frac{L^2}{16A_t} \times 100 \quad (7)$$

Where L [mm] is the perimeter of the square inside of a printed grid and $A_t$ $[\mathrm{mm}^2]$ corresponds to the theoretical area of the square inside of a printed grid. Ideally, Pg =100 %, indicating perfectly square-shaped pores [45, 47].

Additionally, the printed straight lines were used to determine the accuracy of the printing in relation to the size of the nozzle used, and the spreading phenomenon occurring upon material deposition [48, 49]. For this, we calculated strand accuracy according to equation 8.

$$Strand\ accuracy = \frac{D_{nom}}{D_{exp}} \times 100 \quad (8)$$

Where $D_{nom}$ [µm] is the nominal diameter of the nozzle used for printing (here 25 G = 250 µm), $D_{exp}$ [µm] is the diameter of the extruded strand. Ideally, A=100 %, indicating the printed strand diameter same as the diameter of the nozzle used [50].

### 2.14 Statistical analysis

All experiments were carried out in triplicates, and the results were expressed as means ± standard deviations. Statistical analyses were performed using GraphPad Prism 8 (GraphPad Software Inc.) Using one-way ANOVA followed by Tukey's post hoc tests. P-values < 0.05 were considered statistically significant.

## 3 Results and discussion

### 3.1 NMR analysis

Introducing phenol groups to the HA backbone allows for inducing gel formation by employing photocrosslinking mechanisms [27]. Using photosensitizers and exposition to the light with a wavenumber at 405nm enables photocrosslinking leading to covalent and temperature-irreversible gelation [33, 34]. The characteristic peaks at 6.7–7.2 ppm, attributed to the conjugated phenol groups of Ty in the HA backbone, revealed the success of the reaction (Figure 1a(2)), which agrees with existing reports [51, 52].

The degree of substitution with Ty based on $^1$H NMR was estimated at 4.8% [52]. Moreover, the functional grafting of HA with Ty was proven by the formation of a gel upon visible light photopolymerization with Riboflavin/SPS system [27].

To confirm the amination of HA-Ty with ethylenediamine, $^1$H NMR was performed on HA-Ty-$NH_2$ (Figure 1a(3)). Since the amination of HA and conjugation of Ty on HA occur via the reaction of carboxylic groups of HA. The methyl groups of HA do not contribute to the reactions, the peak at 2.04 ppm, which is labeled with A, is related to the protons of methyl groups of HA and was used as the reference peak to calculate the substitution degrees. The protons on the sugar rings of HA in $^1$H NMR spectra of HA-Ty illustrated the signals from 3.36 to 3.87 ppm. The sharp peak at 4.74 ppm is assigned to the solvent ($D_2O$). The conjugation of ethylenediamine on HA occurred via activation of the primary amine using EDC/NHS and reaction with the carboxylic groups. The appearance of two peaks at 2.90ppm and 3.12ppm related to the four protons of ethylenediamine at two different places (which are labeled with C and D in Figure 1a(3)) attest to the successful amination of HA-Ty. Moreover, after the conjugation, the peaks assigned to sugar rings of HA-Ty-$NH_2$ showed a slight shift (from 3.39 to 3.85 ppm), while other peaks were constant. Similarly, it has been reported that conjugation of ethylenediamine on HA changes the location of the protons of the sugar rings of HA and exhibits two new peaks before the sugar rings' peaks [29]. The percentage of 23.51% substitution degree was calculated by comparing the integration of the peaks related to ethylenediamine with the integration of the peak related to the methyl groups of HA as a reference peak with $^1$H NMR.

The activated free primary amine by NHS/EDC formed a covalence bond with carboxylic acid groups of the peptide. The presence of the conjugated peptide was confirmed by the appearance of some new peaks in different ranges (such as from 0.79 to 1.24 ppm, from 3.29 to 3.77 ppm, and from 7.12 to 7.59 ppm) and at 1.93 ppm (Figure 1 a(4)). In peptide-conjugated HA (Figure 1a(4)), the peaks assigned to the protons of methyl groups shifted to 1.99 ppm from 2.04 ppm and the peaks related to the protons on the sugar rings of HA moved to 3.29-3.77 ppm from 3.39 to 3.85 ppm compared to their location in $^1$H NMR of HA-Ty-$NH_2$. The characteristic peak related to protons of ethylenediamine, which was located at 2.90, which is marked with C in Figure1, transformed to 2.77ppm, while another peak, which was at 3.12 ppm in $^1$H NMR of HA-Ty-$NH_2$ (marked with D), overlapped with the peaks of peptide and sugar rings of HA around 3.29 to 3.77 ppm. No shift was not observed in the location of the peaks related to the conjugated ethylenediamine and methyl group in the NMR of HA-Ty-$NH_2$-B, which were located at 2.90, 3.12, and 2.04 ppm.

### 3.2 FTIR spectra of the hydrogels

The FTIR spectra of HA, HA-Ty, and HA-Ty-$NH_2$ are shown in Figure 1 b. The FTIR spectra of the dried hydrogels HA-Ty-$NH_2$-C and HA-Ty-$NH_2$-B and also peptide powder are depicted in Figure 1c. The efficiency of FITR in confirming the reaction between functional groups of two components has been reported by monitoring the intensity and position of peaks related to the functional groups [11, 53]. Although the spectrum of HA-Ty was largely similar to the FTIR spectra of HA, by converting carboxylic bonds to N-H bonds, the peak of carbonyl groups slightly moved from 1604$cm^{-1}$ to 1608$cm^{-1}$. Similarly, it has been reported that the FTIR spectra of HA-Ty remain similar to the spectrum of HA after conjugating Ty on HA [54]. The FTIR spectra of amination HA-Ty showed a new peak assigned to amine groups of ethylenediamine at 3280$cm^{-1}$ [29].

By adding peptides to the structure of the hydrogels either by conjugating or blending, the peak related to the N-H and N-$H_2$ became dominant compared to the peak of hydroxyl groups that appeared at 3276$cm^{-1}$. The conjugation of the peptide on HA-Ty-$NH_2$ via the reaction between carboxyl and amine groups leads to transformation at a wavenumber of carbonyl from 1601$cm^{-1}$ in HA-Ty-$NH_2$ to 1617$cm^{-1}$ in HA-Ty-$NH_2$-C. In comparison, the carbonyl peak of HA-Ty-$NH_2$-B moved to 1604$cm^{-1}$. The peak related to the carbonyl groups shifted more by conjugation than blending since the physical interactions are weaker than chemical bonds. Therefore, the FTIR results of the hydrogels confirmed the results of $^1$H NMR.

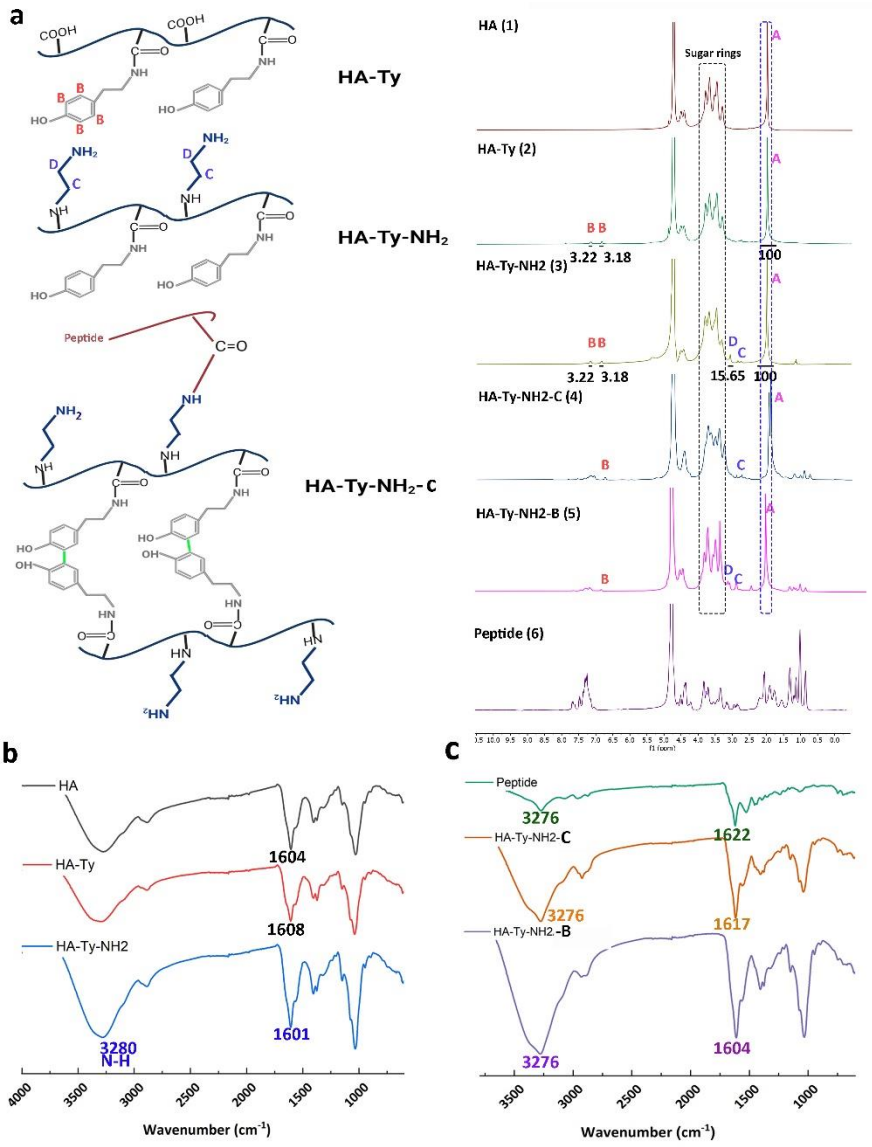


Figure 1. Formula and $^{1}$H NMR spectra (a); FTIR spectra of HA, HA-Ty, HA-Ty-$NH_2$, HA-Ty-$NH_2$-C, HA-Ty-$NH_2$-B, and peptide (b) and (c).

### 3.3 Physical properties of the hydrogels

The physical properties of the HA-Ty-$NH_2$-Chydrogels, such as form (Figure 2a), porosity, swelling, and hydrolytic degradation, which may affect peptide release, cell adhesion, viability, and moisture absorption, were investigated. The porosity of the samples were around 70%.

The swelling behavior of the hydrogels was investigated (Figure 2b) for three days. The blended and conjugated peptide samples increased the swelling rate and ultimate water uptake so that the final weight of HA-Ty-$NH_2$-C and HA-Ty-$NH_2$-B hydrogels were more than 900% of their initial weight, while the

ultimate percentage of water uptake of HA-Ty-$NH_2$ hydrogel after 72h was around 600% (Figure 2b). A faster swelling ratio was observed for HA-Ty-$NH_2$-B compared to HA-Ty-$NH_2$-C and HA-Ty-$NH_2$ in the first five hours. However, after five hours of swelling, the water uptake rate of the blended hydrogels was lower than that of the conjugated hydrogel. It was hypothesized that a rapid release of the peptide containing amino acids with polar groups from the blended hydrogel within five hours decreased the hydrophilicity of the HA-Ty-$NH_2$-B compared to the hydrophilicity of the HA-Ty-$NH_2$-C.

To prove the claim of the burst release of the peptide from HA-Ty-$NH_2$-B hydrogel, the ability of the hydrogels to conserve water over time was studied (Figure 2c). The rate of losing water for HA-Ty-$NH_2$-B at the first 5h was higher than HA-Ty-$NH_2$-C, which might be due to the release of the peptide from the hydrogel during the swelling. The slighter decrease in the water retention ratio of HA-Ty-$NH_2$-C hydrogels can be due to the trapping of the water molecules in the hydrogel structure via the formation of polar bonds and limiting water evaporation.

It is worth mentioning that the hydrolytic degradations were assessed after two days of soaking the hydrogels in PBS (pH of 7.4 and temperature of 37.5°C) since the weight of the hydrogel remained constant after 48h in the swelling test. The degradation of the hydrogels followed the same pattern as swelling (Figure 2d). The presence of the peptide decreased the stability of HA-Ty-$NH_2$ hydrogel, so HA-Ty-$NH_2$-C and HA-Ty-$NH_2$-B hydrogels degraded (dissolved) on day five. A higher swelling of HA-Ty-$NH_2$-B and HA-Ty-$NH_2$-C hydrogels than HA-Ty-$NH_2$ hydrogel due to polar groups of the peptide might increase the force on the crosslinked sites via increasing the number of molecules of water within the hydrogels that, leads to faster degradation. The same trend has been reported for increasing the rate of water uptake and degradation of hydrogels by increasing the concentration of peptides [15].

### 3.4 Rheological investigation

The effect of chemical and physical peptide incorporation on the viscoelastic properties of the HA hydrogel was evaluated using rheological investigation (Figures 2e and f). The frequency sweep result (Figure 2e) demonstrated a frequency independent of G' and G" for the hydrogel indicating the covalent bonding after the photocrosslinking [36, 55]. Moreover, the peptide incorporation did not affect the viscoelastic properties of the hydrogel. At the frequency of 1 Hz, the storage modulus of HA-Ty, HA-Ty-$NH_2$-B, and HA-Ty-$NH_2$-C was close and in the range of 157-185Pa. Hence, the frequency result exhibited that the peptide incorporation had no effect on the viscoelastic properties of the hydrogels, regardless of the method of conjugation. This phenomenon could be due to the low content of the peptide in the hydrogel, as well as its low molecular weight (1 kDa).

Furthermore, like the frequency sweep, the amplitude sweep test revealed no difference among the hydrogel (Figure 2f). Moreover, all hydrogel samples exhibited a similar critical strain at around 500 %, which G' and G" crossed, showing a gel-sol transition of the hydrogel. The viscosity of the HA-Ty-$NH_2$, HA-Ty-$NH_2$-B, and HA-Ty-$NH_2$-C hydrogel precursors containing RF and SPS before photocrosslinking and after photocrosslinking (hydrogel) between shear rate of 0.001 to 1000 1/s were investigated to determined the effect of the crosslinking on the viscosities (Figure 4g,h). The viscosity of the precursors and hydrogels was decreased by increasing the shear rate. However, the viscosity of the gel precursor was $10^3$ times lower than the viscosity of the hydrogels post crosslinking.

### 3.5 Morphology of the hydrogels

To study the microstructure of HA-Ty-$NH_2$ base hydrogels and the effect of the peptide on the morphology of the hydrogels, the morphology of the cross-section of HA-Ty-$NH_2$, HA-Ty-$NH_2$-C, and HA-Ty-$NH_2$-B hydrogels were investigated by SEM micrographs (Figure 2i-k). The results showed no difference in the morphology of the hydrogels. All the samples showed a microporous structure and similar pore sizes. SEM results showed that the peptide's conjugation on HA-Ty-$NH_2$ had no effects, such as decreasing pore size and porosity, which are vital features for the absorption of wound exudate and delivery nutrition to the cells, on the structure of the hydrogels [56].

### 3.6 Peptide release measurement

Figure 2l shows the cumulative peptide release from HA-Ty-$NH_2$, HA-Ty-$NH_2$-C, and HA-Ty-$NH_2$-B hydrogels. The blended hydrogel showed a burst release in the first 6h, with 69±3.6% of the peptides released after 6h. This fast release could be due to a lack of chemical interactions with HA-Ty-$NH_2$. The release continued at a lower rate than the initial burst release from the HA-Ty-$NH_2$-B hydrogel for six days so that the ultimate cumulative concentration of the peptide was 84±2.8%. The chemical interactions between carboxylic groups of the peptide and amine groups of HA-Ty-$NH_2$ postponed the start of release from HA-Ty-$NH_2$-C hydrogel for 12h. After that, the peptide concentration increased at a relatively constant rate in the media (PBS with pH of 7.4) until six days, and the final cumulative concentration reached 53% of the conjugated peptide on HA-Ty-$NH_2$-C hydrogel. The trend of the peptide release from HA-Ty-$NH_2$-C hydrogel followed the pattern of the hydrolytic degradation of the HA-Ty-$NH_2$-C hydrogel. Therefore, the release can be controlled by controlling the degradation of HA-Ty-$NH_2$-C hydrogel.

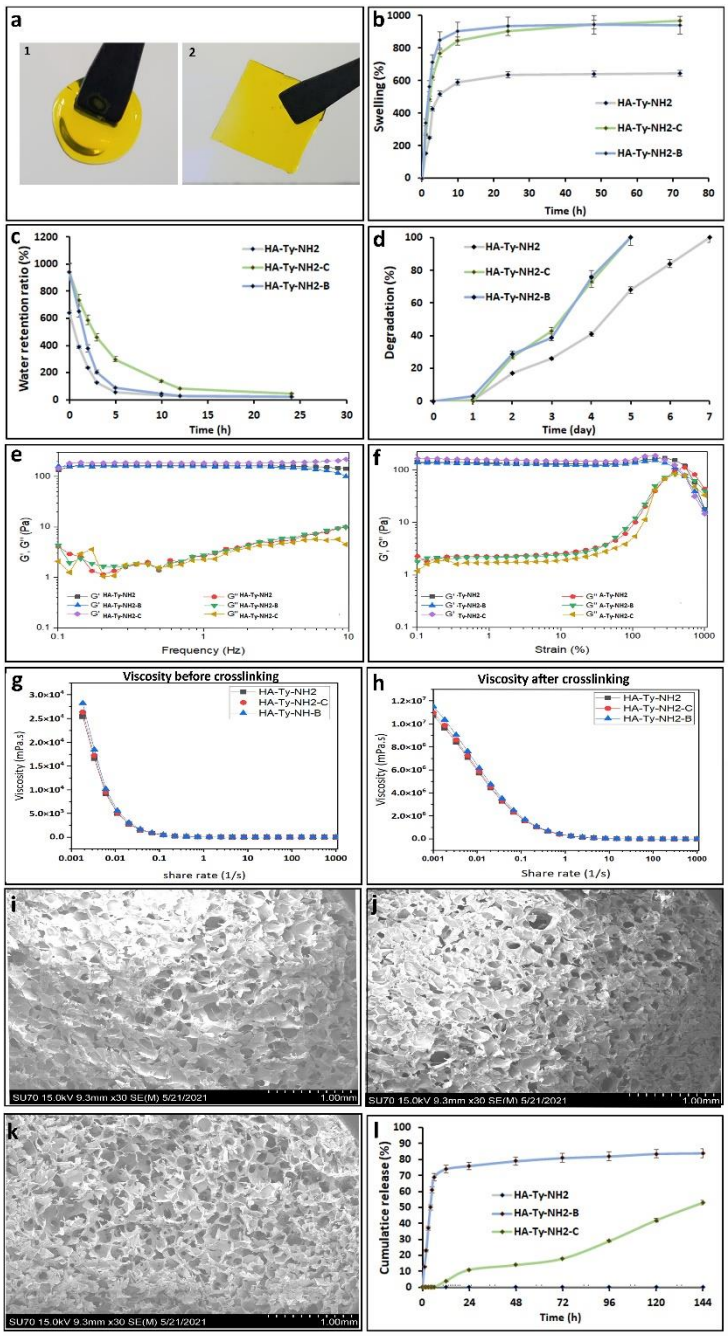


Figure 2. Physical parameters of HA-Ty-$NH_2$, HA-Ty-$NH_2$-C, and HA-Ty-$NH_2$-B, such as form (a), swelling (b), water retention (c), and degradation (d), The rheological properties of HA-Ty hydrogel with chemically and physically peptide of incorporation; (e) storage modulus (G') and loss modulus (G")–frequency dependence of HA-Ty, HA-Ty-$NH_2$/Peptide, and HA-Ty-$NH_2$-Peptide hydrogels at a constant strain of 1%; (f) storage modulus (G') and loss modulus (G")–strain dependence of HA-Ty-$NH_2$, HA-Ty-$NH_2$-B, and HA-Ty-$NH_2$-C hydrogels at a constant frequency of 1 Hz at, viscosity-share rate of the HA-Ty-$NH_2$, HA-Ty-$NH_2$-B, and HA-Ty-$NH_2$-C solution before crosslinking (g), viscosity-share rate of the HA-Ty-$NH_2$, HA-Ty-$NH_2$-B,

and HA-Ty-$NH_2$-C gel (after crosslinking) (h), SEM micrograph images of the cross-section of HA-Ty (i), HA-Ty-$NH_2$-B (j), and HA-Ty-$NH_2$-C (k) hydrogels with magnification X30, and (l) cumulative peptide release of HA-Ty, HA-Ty-$NH_2$-B, and HA-Ty-$NH_2$-C hydrogels.

### 3.7 Cell viability

The cell cytocompatibility of the hydrogels was evaluated using MTS and Live/ Dead cell staining. The conjugated and blended hydrogels were not cytotoxic (Figure 3a). The significant effect of the peptide on cell viability was detected on the first day of MTS evaluation by comparing the percentage of cell viability of HA-Ty-$NH_2$-C and HA-Ty-$NH_2$-B with HA-Ty-$NH_2$ (Figure 3a). However, the difference between the cell viability of the conjugated hydrogels and the blended hydrogels was negligible. The cell viability of the conjugated hydrogel after three and seven days of cell culture was 19 and 14% higher than the control hydrogel (HA-Ty-$NH_2$ hydrogel), respectively, while the percentage of cell viability of the blended hydrogels was lower than the control. According to the release of the peptide from HA-Ty-$NH_2$-B hydrogels, the released peptide could be leached out by changing the cell media and could then not promote cell viability on days three and seven. In contrast, the conjugated hydrogels providing the peptide for seven days increased the viability more than the control and the blended hydrogel. The improvement of cell viability by increasing the peptide has been reported [57, 58]. Therefore, a sustained release of the conjugated peptide via the degradation of hydrogels could enhance cell viability and promote the performance of the peptide.

Performing cell staining after seven days, we were able to observe uniformly distributed cells or small agglomerates, of which only a few cells were dead (Figure 3 b, c, d). Cell agglomeration was observed in the case of the presence of the hydrogels with the peptide. Staining results showed cell adherence to the hydrogels along with high cell viability, indicating the promising prospect of developing peptide-enhanced hydrogel

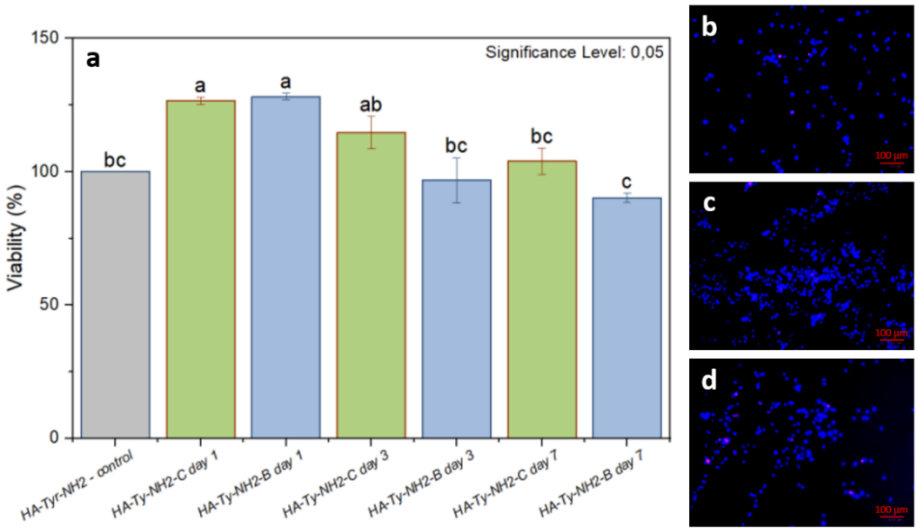


Figure 3. Cell viability results of the hydrogels based on: HA-Ty-$NH_2$, HA-Ty-$NH_2$-C, and HA-Ty-$NH_2$-B (a). Results are expressed as % cell viability and are the mean ± SD of three independent experiments. Micrographs show the distribution of all cells (blue) and dead cells (red) on the hydrogels' surface for samples obtained from HA-Ty-$NH_2$ (b), HA-Ty-$NH_2$-C (c), and HA-Ty-$NH_2$-B (d). Columns that do not share the same letter(s) are significantly different.

### 3.8 Printability

The solution of HA is viscous and shear-thinning but lacks shape retention and is not printable [59]. Hence, to synthesize a printable HA, HA usually is mixed with a self-standing material or multiple chemical derivatives to give shear thinning properties or the ability for post-printing crosslinking [59]. Wang *et al.* synthesized an injectable HA via conjugation Ty on the backbone of HA and enzymatic crosslinking to deliver peptides for promoting the formation of functional vasculature [60]. The printability of the conjugated peptide on HA-Ty-$NH_2$ hydrogel by post-photocrosslinking approach was investigated. As seen in Figure 4, HA-Ty-$NH_2$-C hydrogels could easily be printed in different shapes. The printability and stable structure during HA-Ty printing have been proven in several works [60, 61]. Resolution in extrusion printing is a complex issue as it is affected by printing pressure, nozzle size and shape, printing speed, and viscoelastic properties of the material. To provide a quantitative measure for the printability of our hydrogel precursors in Figures 4a and b, pore squareness and strand accuracy determined based on the images of printed grids and lines. More circular pores and lower pore squareness were observed for the peptide conjugated hydrogels. Pore squareness of HA-Ty-$NH_2$-C was 79.98 ± 3.08. Achieving 100 % of pore squareness is impossible when printing with soft-hydrogel materials, due to two inevitable reasons. The width of the hydrogel strand becomes larger than the nozzle size [7] and the area where strands are

deposited one on another flattens due to the soft nature of the materials used in extrusion printing [4, 6]. While printing the lines (Figure 4b) we were able to obtain uniform strands, but concomitantly the material spreadability damaged the strand accuracy [8].

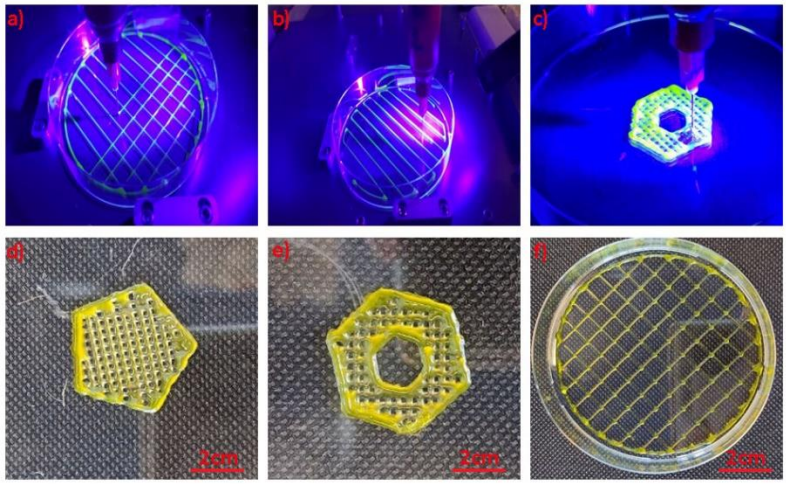


Figure 4. (a-f) Different objects were 3D printed using HA-Ty-$NH_2$-C, and photo-crosslinking was triggered by exposing the objects to UV light.

## 4 Conclusion

The VW-9 peptide was conjugated on aminated HA-Ty via interaction between the primary amine of ethylenediamine of HA-Ty-$NH_2$ and the carboxylic acid of the peptide. Incorporating the peptide into the HA-Ty-$NH_2$ hydrogel either via conjugation or blending increased the swelling capacity, and accelerated hydrolytic degradation of the hydrogels. The conjugated peptide could decrease the rate of water evaporation from HA-Ty-$NH_2$-C hydrogel due to the weak interaction of hydrophilic groups of the peptide with molecules of water, while in the blended hydrogel, the ratio of water evaporation was higher than conjugated hydrogel due to rapid release of peptide and diminishing of polar groups. However, the presence of the peptide in the structure of the hydrogels did not change the rheological properties and morphology of the hydrogels. HA-Ty-$NH_2$-B hydrogels released 69% of the incorporated peptides in the first six h. The conjugated hydrogel showed better cell viability on days 3 and 7 compared to the blended hydrogel. The hydrogel was printed with different geometry to evaluate their potential to design various wound dressings.

**Funding**

This research work was supported by grants from the Fonds National de la Recherche Scientific de Belgique (FNRS) (grant number 38351, 2021 awarded to Pejman Ghaffari-Bohlouli, and 46599, 2022 awarded to Julia Simińska-Stanny) and Innoviris Brussels, Belgium (under the project 2019-BRIDGE-4: RE4BRU).

## References

[1] W. Ahn, J.-H. Lee, S.R. Kim, J. Lee, E.J. Lee, Designed protein- and peptide-based hydrogels for biomedical sciences, Journal of Materials Chemistry B 9(8) (2021) 1919-1940.
[2] P. Ghaffari-Bohlouli, H. Jafari, N. Taebnia, A. Abedi, A. Amirsadeghi, S.V. Niknezhad, H. Alimoradi, S. Jafarzadeh, M. Mirzaei, L. Nie, Protein by-products: Composition, extraction, and biomedical applications, Critical reviews in food science and nutrition (2022) 1-46.
[3] S. Das, D. Das, Rational Design of Peptide-based Smart Hydrogels for Therapeutic Applications, Frontiers in Chemistry 9 (2021).
[4] T. Guan, J. Li, C. Chen, Y. Liu, Self-Assembling Peptide-Based Hydrogels for Wound Tissue Repair, Advanced Science 9(10) (2022) 2104165.
[5] Z. Zhai, K. Xu, L. Mei, C. Wu, J. Liu, Z. Liu, L. Wan, W. Zhong, Co-assembled supramolecular hydrogels of cell adhesive peptide and alginate for rapid hemostasis and efficacious wound healing, Soft Matter 15(42) (2019) 8603-8610.
[6] T. Cui, X. Li, S. He, D. Xu, L. Yin, X. Huang, S. Deng, W. Yue, W. Zhong, Instant Self-Assembly Peptide Hydrogel Encapsulation with Fibrous Alginate by Microfluidics for Infected Wound Healing, ACS Biomaterials Science & Engineering 6(9) (2020) 5001-5011.
[7] Y. Loo, Y.-C. Wong, E.Z. Cai, C.-H. Ang, A. Raju, A. Lakshmanan, A.G. Koh, H.J. Zhou, T.-C. Lim, S.M. Moochhala, C.A.E. Hauser, Ultrashort peptide nanofibrous hydrogels for the acceleration of healing of burn wounds, Biomaterials 35(17) (2014) 4805-4814.
[8] M. Mirzaei, A. Shavandi, G. Dodi, I. Gardikiotis, S.-A. Pasca, S. Mirdamadi, N. Soleymanzadeh, H. Alimoradi, M. Moser, S. Goriely, A Yeast-Derived Peptide Promotes Skin Wound Healing by Stimulating Effects on Fibroblast and Immunomodulatory Activities, SSRN Electronic Journal (2022).
[9] M. Mirzaei, S. Mirdamadi, M.R. Ehsani, M. Aminlari, Production of antioxidant and ACE-inhibitory peptides from Kluyveromyces marxianus protein hydrolysates: Purification and molecular docking, Journal of Food and Drug Analysis 26(2) (2018) 696-705.
[10] Q. Gao, Y. He, J.Z. Fu, A. Liu, L. Ma, Coaxial nozzle-assisted 3D bioprinting with built-in microchannels for nutrients delivery, Biomaterials 61 (2015) 203-15.
[11] M. Rozenberg, S. Lansky, Y. Shoham, G. Shoham, Spectroscopic FTIR and NMR study of the interactions of sugars with proteins, Spectrochimica Acta Part A: Molecular and Biomolecular Spectroscopy 222 (2019) 116861.
[12] E.C. González-Díaz, S. Varghese, Hydrogels as Extracellular Matrix Analogs, Gels 2(3) (2016).
[13] I. Firlar, M. Altunbek, C. McCarthy, M. Ramalingam, G. Camci-Unal, Functional Hydrogels for Treatment of Chronic Wounds, Gels 8(2) (2022).
[14] H. Jafari, P. Ghaffari, V. Niknezhad, A. Abedi, Z. Izadifar, R. Mohammadinejad, R.S. Varma, A. Shavandi, Tannic acid: a versatile polyphenol for design of biomedical hydrogels, Journal of Materials Chemistry B (2022).

[15] J. Zhu, H. Han, F. Li, X. Wang, J. Yu, X. Qin, D. Wu, Peptide-functionalized amino acid-derived pseudoprotein-based hydrogel with hemorrhage control and antibacterial activity for wound healing, Chemistry of Materials 31(12) (2019) 4436-4450.
[16] B. Hu, M. Gao, K.O. Boakye-Yiadom, W. Ho, W. Yu, X. Xu, X.-Q. Zhang, An intrinsically bioactive hydrogel with on-demand drug release behaviors for diabetic wound healing, Bioactive materials 6(12) (2021) 4592-4606.
[17] P. Ghaffari-Bohlouli, F. Hamidzadeh, P. Zahedi, M. Shahrousvand, M. Fallah-Darrehchi, Antibacterial nanofibers based on poly (l-lactide-co-d, l-lactide) and poly (vinyl alcohol) used in wound dressings potentially: A comparison between hybrid and blend properties, Journal of Biomaterials Science, Polymer Edition 31(2) (2020) 219-243.
[18] O. Tsur-Gang, E. Ruvinov, N. Landa, R. Holbova, M.S. Feinberg, J. Leor, S. Cohen, The effects of peptide-based modification of alginate on left ventricular remodeling and function after myocardial infarction, Biomaterials 30(2) (2009) 189-195.
[19] M. Ghosh, M. Halperin-Sternfeld, I. Grinberg, L. Adler-Abramovich, Injectable alginate-peptide composite hydrogel as a scaffold for bone tissue regeneration, Nanomaterials 9(4) (2019) 497.
[20] B. Hu, S. Wang, J. Li, X. Zeng, Q. Huang, Assembly of bioactive peptide–chitosan nanocomplexes, The Journal of Physical Chemistry B 115(23) (2011) 7515-7523.
[21] S.T. Koshy, D.K. Zhang, J.M. Grolman, A.G. Stafford, D.J. Mooney, Injectable nanocomposite cryogels for versatile protein drug delivery, Acta biomaterialia 65 (2018) 36-43.
[22] B. Layek, L. Lipp, J. Singh, Cell penetrating peptide conjugated chitosan for enhanced delivery of nucleic acid, International journal of molecular sciences 16(12) (2015) 28912-28930.
[23] M. Mochizuki, Y. Kadoya, Y. Wakabayashi, K. Kato, I. Okazaki, M. Yamada, T. Sato, N. Sakairi, N. Nishi, M. Nomizu, Laminin-1 peptide-conjugated chitosan membranes as a novel approach for cell engineering, The FASEB journal 17(8) (2003) 1-20.
[24] F. Della Sala, G. Longobardo, A. Fabozzi, M. di Gennaro, A. Borzacchiello, Hyaluronic acid-based wound dressing with antimicrobial properties for wound healing application, Applied Sciences 12(6) (2022) 3091.
[25] Y.-W. Ding, Z.-Y. Wang, Z.-W. Ren, X.-W. Zhang, D.-X. Wei, Advances in modified hyaluronic acid-based hydrogels for skin wound healing, Biomaterials Science (2022).
[26] A. Shavandi, G. Dodi, I. Gardikiotis, S.-A. Pasca, S. Mirdamadi, N. Soleymanzadeh, H. Alimoradi, M. Moser, S. Goriely, A Yeast-Derived Peptide Promotes Skin Wound Healing by Stimulating Effects on Fibroblast and Immunomodulatory Activities.
[27] B.M. Hong, S.A. Park, W.H. Park, Effect of photoinitiator on chain degradation of hyaluronic acid, Biomaterials Research 23(1) (2019) 1-8.
[28] R. Ziadlou, S. Rotman, A. Teuschl, E. Salzer, A. Barbero, I. Martin, M. Alini, D. Eglin, S. Grad, Optimization of hyaluronic acid-tyramine/silk-fibroin composite hydrogels for cartilage tissue engineering and delivery of anti-inflammatory and anabolic drugs, Materials Science and Engineering: C 120 (2021) 111701.
[29] T.N. Thanh, N. Laowattanatham, J. Ratanavaraporn, A. Sereemaspun, S. Yodmuang, Hyaluronic acid crosslinked with alginate hydrogel: A versatile and biocompatible bioink platform for tissue engineering, European Polymer Journal 166 (2022) 111027.
[30] H. Tan, H. Li, J.P. Rubin, K.G. Marra, Controlled gelation and degradation rates of injectable hyaluronic acid-based hydrogels through a double crosslinking strategy, Journal of tissue engineering and regenerative medicine 5(10) (2011) 790-797.
[31] C.-H. Zheng, J.-Q. Gao, Y.-P. Zhang, W.-Q. Liang, A protein delivery system: biodegradable alginate–chitosan–poly (lactic-co-glycolic acid) composite microspheres, Biochemical and Biophysical Research Communications 323(4) (2004) 1321-1327.

[32] P.E. Donnelly, T. Chen, A. Finch, C. Brial, S.A. Maher, P.A. Torzilli, Photocrosslinked tyramine-substituted hyaluronate hydrogels with tunable mechanical properties improve immediate tissue-hydrogel interfacial strength in articular cartilage, Journal of Biomaterials science, Polymer edition 28(6) (2017) 582-600.
[33] I.A. Barroso, K. Man, T.E. Robinson, S.C. Cox, A.K. Ghag, Photocurable GelMA Adhesives for Corneal Perforations, Bioengineering (Basel) 9(2) (2022).
[34] R. Goto, E. Nishida, S. Kobayashi, M. Aino, T. Ohno, Y. Iwamura, T. Kikuchi, J.-I. Hayashi, G. Yamamoto, M. Asakura, A. Mitani, Gelatin Methacryloyl-Riboflavin (GelMA-RF) Hydrogels for Bone Regeneration, International journal of molecular sciences 22(4) (2021) 1635.
[35] Z. Ahmadian, A. Correia, M. Hasany, P. Figueiredo, F. Dobakhti, M.R. Eskandari, S.H. Hosseini, R. Abiri, S. Khorshid, J. Hirvonen, A hydrogen-bonded extracellular matrix-mimicking bactericidal hydrogel with radical scavenging and hemostatic function for pH-responsive wound healing acceleration, Advanced healthcare materials 10(3) (2021) 2001122.
[36] H. Jafari, P. Ghaffari-bohlouli, D. Podstawczyk, L. Nie, A. Shavandi, Tannic acid post-treatment of enzymatically crosslinked chitosan-alginate hydrogels for biomedical applications, Carbohydrate Polymers 295 (2022) 119844.
[37] S. Yan, G. Han, Q. Wang, S. Zhang, R. You, Z. Luo, A. Xu, X. Li, M. Li, Q. Zhang, Directed assembly of robust and biocompatible silk fibroin/hyaluronic acid composite hydrogels, Composites Part B: Engineering 176 (2019) 107204.
[38] H. Jafari, C. Delporte, K.V. Bernaerts, H. Alimoradi, L. Nie, D. Podstawczyk, K.C. Tam, A. Shavandi, Synergistic complexation of phenol functionalized polymer induced in situ microfiber formation for 3D printing of marine-based hydrogels, Green Chemistry 24(6) (2022) 2409-2422.
[39] X. Liu, B. Yu, Q. Huang, R. Liu, Q. Feng, Q. Cai, S. Mi, In vitro BMP-2 peptide release from thiolated chitosan based hydrogel, International journal of biological macromolecules 93 (2016) 314-321.
[40] H. Jafari, H. Alimoradi, C. Delporte, K.V. Bernaerts, R. Heidari, D. Podstawczyk, S.V. Niknezhad, A. Shavandi, An injectable, self-healing, 3D printable, double network co-enzymatically crosslinked hydrogel using marine poly-and oligo-saccharides for wound healing application, Applied Materials Today 29 (2022) 101581.
[41] F. Maleki, H. Jafari, P. Ghaffari-bohlouli, M. Shahrousvand, G.M.M. Sadeghi, H. Alimoradi, A. Shavandi, Proliferation and osteogenic differentiation of mesenchymal stem cells on three-dimensional scaffolds made by thermal sintering method, Chemical Papers 75(11) (2021) 5971-5981.
[42] P. Ghaffari-Bohlouli, P. Zahedi, M. Shahrousvand, Enhanced osteogenesis using poly (l-lactide-co-d, l-lactide)/poly (acrylic acid) nanofibrous scaffolds in presence of dexamethasone-loaded molecularly imprinted polymer nanoparticles, International Journal of Biological Macromolecules 165 (2020) 2363-2377.
[43] N. Parekh, C. Hushye, S. Warunkar, S. Gupta, A. Nisal, In vitro study of novel microparticle based silk fibroin scaffold with osteoblast-like cells for load-bearing osteo-regenerative applications †, RSC Adv. 7 (2017) 26551-26558.
[44] C.A. Schneider, W.S. Rasband, K.W. Eliceiri, NIH Image to ImageJ: 25 years of image analysis, Nature Methods 9(7) (2012) 671-675.
[45] H. Jongprasitkul, S. Turunen, V.S. Parihar, M. Kellomäki, Two-step crosslinking to enhance the printability of methacrylated gellan gum biomaterial ink for extrusion-based 3D bioprinting, Bioprinting 25 (2022) e00185.
[46] L. Ouyang, R. Yao, Y. Zhao, W. Sun, Effect of bioink properties on printability and cell viability for 3D bioplotting of embryonic stem cells, Biofabrication 8(3) (2016) 035020.
[47] S. Naghieh, X. Chen, Printability–A key issue in extrusion-based bioprinting, Journal of Pharmaceutical Analysis 11(5) (2021) 564-579.

[48] R. Suntornnond, E. Tan, J. An, C. Chua, A Mathematical Model on the Resolution of Extrusion Bioprinting for the Development of New Bioinks, Materials 9 (2016) 756.
[49] G. Gillispie, P. Prim, J. Copus, J. Fisher, A.G. Mikos, J.J. Yoo, A. Atala, S.J. Lee, Assessment methodologies for extrusion-based bioink printability, Biofabrication 12(2) (2020) 022003.
[50] T. Gao, G.J. Gillispie, J.S. Copus, A.K. Pr, Y.J. Seol, A. Atala, J.J. Yoo, S.J. Lee, Optimization of gelatin-alginate composite bioink printability using rheological parameters: a systematic approach, Biofabrication 10(3) (2018) 034106.
[51] S. Sakai, T. Kotani, R. Harada, R. Goto, T. Morita, S. Bouissil, P. Dubessay, G. Pierre, P. Michaud, R. El Boutachfaiti, M. Nakahata, M. Kojima, E. Petit, C. Delattre, Development of phenol-grafted polyglucuronic acid and its application to extrusion-based bioprinting inks, Carbohydrate Polymers 277 (2022) 118820.
[52] C. Loebel, M. D'Este, M. Alini, M. Zenobi-Wong, D. Eglin, Precise tailoring of tyramine-based hyaluronan hydrogel properties using DMTMM conjugation, Carbohydrate Polymers 115 (2015) 325-333.
[53] C. Cateto, M. Barreiro, A. Rodrigues, Monitoring of lignin-based polyurethane synthesis by FTIR-ATR, industrial crops and products 27(2) (2008) 168-174.
[54] R. Egbu, S. Brocchini, P.T. Khaw, S. Awwad, Antibody loaded collapsible hyaluronic acid hydrogels for intraocular delivery, European Journal of Pharmaceutics and Biopharmaceutics 124 (2018) 95-103.
[55] D.E. Apostolides, C.S. Patrickios, Dynamic covalent polymer hydrogels and organogels crosslinked through acylhydrazone bonds: Synthesis, characterization and applications, Polymer International 67(6) (2018) 627-649.
[56] T. Tokatlian, C. Cam, T. Segura, Porous hyaluronic acid hydrogels for localized nonviral DNA delivery in a diabetic wound healing model, Advanced healthcare materials 4(7) (2015) 1084-1091.
[57] K. Roy, G. Pandit, M. Chetia, A.K. Sarkar, S. Chowdhuri, A.P. Bidkar, S. Chatterjee, Peptide Hydrogels as Platforms for Sustained Release of Antimicrobial and Antitumor Drugs and Proteins, ACS Applied Bio Materials 3(9) (2020) 6251-6262.
[58] K. Kulkarni, R.L. Minehan, T. Gamot, H.A. Coleman, S. Bowles, Q. Lin, D. Hopper, S.E. Northfield, R.A. Hughes, R.E. Widdop, M.-I. Aguilar, H.C. Parkington, M.P. Del Borgo, Esterase-Mediated Sustained Release of Peptide-Based Therapeutics from a Self-Assembled Injectable Hydrogel, ACS Applied Materials & Interfaces 13(49) (2021) 58279-58290.
[59] D. Petta, U. D'amora, L. Ambrosio, D. Grijpma, D. Eglin, M. D'este, Hyaluronic acid as a bioink for extrusion-based 3D printing, Biofabrication 12(3) (2020) 032001.
[60] L.-S. Wang, F. Lee, J. Lim, C. Du, A.C. Wan, S.S. Lee, M. Kurisawa, Enzymatic conjugation of a bioactive peptide into an injectable hyaluronic acid–tyramine hydrogel system to promote the formation of functional vasculature, Acta biomaterialia 10(6) (2014) 2539-2550.
[61] K. Flégeau, A. Puiggali-Jou, M. Zenobi-Wong, Cartilage tissue engineering by extrusion bioprinting utilizing porous hyaluronic acid microgel bioinks, Biofabrication 14(3) (2022) 034105.
[62] G. Tan, J. Xu, Q. Yu, J. Zhang, X. Hu, C. Sun, H. Zhang, Photo-Crosslinkable Hydrogels for 3D Bioprinting in the Repair of Osteochondral Defects: A Review of Present Applications and Future Perspectives, Micromachines (Basel) 13(7) (2022).
[63] A.C. Daly, S.E. Critchley, E.M. Rencsok, D.J. Kelly, A comparison of different bioinks for 3D bioprinting of fibrocartilage and hyaline cartilage, Biofabrication 8(4) (2016) 045002.
[64] J. Göhl, K. Markstedt, A. Mark, K. Håkansson, P. Gatenholm, F. Edelvik, Simulations of 3D bioprinting: predicting bioprintability of nanofibrillar inks, Biofabrication 10(3) (2018) 034105.